Viscosity in Keplerian Disks: Steady-State Velocity Distribution and Non-Local Collision Effects

J.M. Petit
C.N.R.S., Observatoire de Nice, France
&
Lunar and Planetary Laboratory
University of Arizona
Tucson, AZ 85721
petit@bach.obs-nice.fr

Richard Greenberg
Lunar and Planetary Laboratory
University of Arizona
Tucson, AZ 85721
Phone: 602-621-6940
FAX: 602-621-5133
greenberg@lpl.arizona.edu

Submitted to Icarus
Dec 23, 1994
Revised Nov 8, 1995
Revised again Feb 16, 1996

Number of manuscript pages: 17
Number of figures: 8 (some are multi-part for a total of 13)
Number of tables: 2

Keywords: Planetary Rings
Celestial Mechanics
Collisional Physics
Impact Processes
Planetary Dynamics

Proposed running title: Viscosity in Keplerian Disks

Send proofs to:

Richard Greenberg
Lunar and Planetary Laboratory
University of Arizona
Tucson, AZ, 85721
Phone: 602-621-6940
FAX: 602-621-5133
greenberg@lpl.arizona.edu

Abstract

A kinetic model based on a numerical algorithm, rather than Boltzman's equation, yields the viscosity and velocity distribution for colliding, finite-size particles in a planetary ring. Results are similar to those of many-particle simulations, and show that non-local effects due to the finite size are dominant in many cases of interest. Only for small particles does the viscosity decrease with increasing optical thickness sufficiently for the standard ringlet instability model to apply. This numerical kinetic theory will allow study of multi-size particle distributions, as well as scattering due to gravitational interactions or alternative collision models.

I Introduction

Angular momentum transport is a key process driving the large-scale structure of planetary rings. It determines the time-scale for radial spreading, which is remarkably short in the case of Saturn's rings, and the behavior of wave structures. Analytical studies of momentum transport generally follow traditional formulations of statistical mechanics, with modified versions of Boltzman's equation representing the dynamics in a keplerian swarm of particles (Goldreich and Tremaine 1978, Shu and Stewart 1985, Araki and Tremaine 1986). Such approaches often involve complicated mathematics that can obscure the underlying physical processes and make the modeling of critical collisional effects difficult to evaluate.

Greenberg (1988) took a more heuristic and physical approach which led to results similar to earlier analyses. Greenberg's approach was used by Ojakangas and Greenberg (1990) to examine momentum transport in the case of a disk or planetary ring with a radial surface density gradient. The general approach involves estimating the concurrent redistribution of velocity due to collisions and due to keplerian motion. The collisions tend to reduce orbital eccentricities due to the effect of impact energy loss on relative velocities; collisions may also tend to increase some eccentricities as scattering creates a more isotropic relative-velocity distribution relative to the elliptical distribution associated with swarms of orbiting particles. At the same time keplerian motion tends to drive an isotropic distribution toward a distribution with an excess of radial velocity components. Modeling these competing effects on velocities gives a steady-state velocity distribution, which in turn can be integrated to find momentum transport and its coefficient, the viscosity ν.

Another approach to study of transport processes has been to construct numerical many-particle simulations in which the actual motion of individual particles is computed and tracked. Simulations by Wisdom and Tremaine (1988) and by Salo (1991) have provided considerable insight into the dynamics of such systems.

In computing viscosity, two components of momentum transport must be taken into account. One component is found by determining (to some level of approximation) the probability distribution of the velocity of particles' centers at a representative point in a model planetary ring. Then the momentum transport is evaluated by integrating over the velocity distribution, weighted by the probability, the angular momentum carried as particles move radially through the test locality. Because this calculation ignores transport by interactions between particles centered at different locations, it yields the so-called "local" component of the viscosity.

However, "non-local" transport must be considered if the particles have significant finite size. Particles centered on opposite sides of a shear plane may collide and transport momentum without their centers actually crossing over. This contribution to the viscosity is potentially important if the particles' sizes approach the scale of their eccentric motion, ae (alternatively called their random or thermal motion by some authors). Similarly, non-local effects must be considered if mutual gravitational effects near encounter are to be included, as well as collisions, in a momentum transport model.

The evaluation of viscosity ν by Goldreich and Tremaine (1978) included only the local component. Their work showed a decrease in ν as the optical thickness τ of the ring increased above unity. That result inspired explanations for the ringlet structure of Saturn's rings, because it was shown to lead to potential ringlet-forming instabilities (Ward 1981, Lin and Bodenheimer 1981). Greenberg's (1988) analysis also only considered the local component of ν.

Araki and Tremaine (1986) did include the non-local transport due to finite-size particles, but they invoked a statistical approach that cannot be readily interpreted in terms of the physics of individual particle collisions. An important result was that ν increases with τ, even for $\tau > 1$. This work showed that non-local effects can be very important, and that they seemed to eliminate the possibility of ringlet instabilities.

The many-particle simulations by Wisdom and Tremaine (1988) and by Salo (1991) yielded similar results, with ring particle radii of 1m. Salo did suggest that reduction of the particle size in the model to 1cm might give the dependence of ν on τ that is required for the ringlet instability.

In this paper, we study the effects of the collisional process using a numerical algorithm that tracks the evolution of the velocity distribution, by statistically taking into account the continual processes of mutual collision among particles and of keplerian motion. The model includes finite-size particles and accounts for both local and non-local transport. The algorithm is based on the physical description of the mechanics by Greenberg (1988). This approach provides great flexiblity in incorporating physical models of the outcomes of collisions, without the constraints of fitting a Boltzman formulation. Moreover, because the Boltzman equation generally has to be solved numerically in any case, it does not really provide any advantage over our algorithmic computation. Our results are complementary to the many-particle simulations, providing statistical results rather than the experiment-specific results of the simulations.

Our formalism is structured to allow eventual inclusion of the effect of gravitation between particles, in cases where Hill's approximation is valid. In principle, a "close encounter" may involve collisions alone in the case without gravitation, or both collisions and gravitation when Hill's approximation applies. Results with gravitational effects will be described in future work; the computational results obtained in this paper involve only collisions. First we describe a two-dimensional ("flat ring") model. Then in Sec. IV, we describe corrections that approximate a three-dimensional model. The results confirm the essential results of the earlier work, and lay the groundwork for inclusion of gravitational encounters and alternative collision models.

II Method of Computation

The local viscosity is a parameter describing the transport of momentum across a boundary, due to particles crossing that boundary. In the case of disks, the relevant boundary is a circle around the central planet. The radial and tangential components of the velocity of particles relative to the circular orbital velocity at a point on that circle are given by V_r and V_t. The momentum transported is proportional to V_t and the rate of transport is proportional to V_r. Hence the rate of transport of momentum is proportional to $\langle V_r V_t \rangle$, which is the key quantity to be evaluated. Viscosity is readily calculated by scaling to the density and systematic velocity shear (e.g. Greenberg 1988).

The non-local transport is due to exchange of angular momentum between pairs of colliding particles, each with one particle centered inside the shear boundary and the other outside. We must then sum over all possible collisions involving such pairs and compute the transfer of angular momentum, which is not included in the calculation of local viscosity.

For both cases (local and non-local), we first need to know the equilibrium velocity distribution in order to determine the frequencies of all the possible collisions and of all boundary crossings. This is done by integrating the equation of evolution of the velocity distribution function which accounts for the keplerian shift and the scattering due to collisions.

We have developed a numerical model that computes the evolution of the velocity distribution in (V_r, V_t) space by taking a series of small time steps, and in each one moving the particles along keplerian paths (the 2/1 ellipses described by Greenberg 1988) and also redistributing them according to collisional statistics. For the keplerian motion we use the epicyclic approximation, i.e. the calculations are first-order in orbital eccentricity. In each time step, the probable number of collisions between every pair of points in (V_r, V_t) space is computed for each time step (see Eq. 2 below), and particles are then redistributed according to a collisional scattering model.

For the cases considered here, in our scattering model the particles are assumed to be solid spheres, and the collisions occur with no tangential friction (i.e. perfectly slippery particles so that relative tangential velocity at the contact point is unchanged). A coefficient of restitution ϵ with a value between 0 and 1 describes the change in the radial component of the relative velocity due to energy loss at impact. In most of our numerical experiments, ϵ is assumed to be a function of impact velocity, according to the data of Bridges et al. (1984). This collisional model is fairly conventional in ring dynamics studies, although some models (unlike ours) compute ϵ from the mean velocity of the system, rather than separately for each impact geometry.

In order to compute the contribution to momentum transport due to collisions between one particle centered on one side of the boundary and another particle centered on the other side (non-local), we account for all possible collisions that transport momentum in this way. We assume initially a two-dimensional model in which every particle is on the same orbital plane. In effect, all collisional dynamics are identical to that of hockey pucks on a plane, or of infinitely long, vertically oriented cylinders. After discussing the results of this two-dimensional case, we will describe modifications that simulate a three-dimensional disk, i.e. one that is thicker than the particle size so that particles can pass above and below one another.

Consider Fig. 1, which shows a particle #1 with its center barely on one side of a shear boundary, being hit by a second particle on the other side. We let r_0 be the distance from the center of the primary to the circular shear boundary under consideration, and R_1 and R_2 are the radii of the particles.

The particles' surface number density is given by

$$N_{surf} = \int_e \int_\theta n(e,\theta) de d\theta, \tag{1}$$

where θ is the mean anomaly of the particle, e is orbital eccentricity, and n the number of particles (per area of the disk) with e, θ. (At any position in the disk, the velocity is characterized by e, θ.) The number of particles #2 hitting #1 during a time dt at an orientation within $d\beta$ of the position β is

$$N_{2,hit} = n(e_2,\theta_2) de_2 d\theta_2 (R_1 + R_2) d\beta |V_v| dt, \tag{2}$$

where V_v is the component of the relative velocity perpendicular to the surface of the particles at the point of contact. From the epicyclic approximation (first order in e) of keplerian motion, V_v is given by:

$$\begin{aligned} V_v &= \Omega_0 r_0 \Bigg[(e_2 \sin(\theta_2) - e_1 \sin(\theta_1)) \sin(\beta) \\ &\quad + \left(e_2 \cos(\theta_2) - e_1 \cos(\theta_1) - 3\frac{R_1 + R_2}{r_0} \sin(\beta) \right) \frac{\cos(\beta)}{2} \Bigg], \end{aligned} \tag{3}$$

where Ω_0 is the keplerian circular angular velocity at r_0.

For any given contact orientation β, a more general momentum-transfer impact might have the two particles at any distance from the primary such that the shear boundary lies between their centers. In Fig. 1, for example, the two particles could be shifted leftward, keeping β constant. The radial distance of particle #1 from the primary can be expressed as:

$$r(\lambda) = r_0 - \lambda(R_1 + R_2) sin(\beta) \tag{4}$$

where the coefficient $(0 > \lambda > 1)$ expresses the position relative to the shear boundary. In Fig 1, λ is very small.

Next consider the change in angular momentum during a collision. Before the impact, the angular momentum of particle #1 is:

$$A_1(r) = \Omega(r) r^2 (1 + \frac{e_1}{2} \cos(\theta_1)). \tag{5}$$

Expanding to first order in the small quantities e and $(r - r_0)/r_0$, we obtain:

$$\Omega(r) = \Omega_0 + (r - r_0) \frac{d\Omega}{dr}(r = r_0)$$

$$
\begin{aligned}
&= \Omega_0\left[1+\frac{3}{2}\lambda\sin(\beta)\frac{R_1+R_2}{r_0}\right] && (6)\\
r^2 &= r_0^2\left[1-2\lambda\sin(\beta)\frac{R_1+R_2}{r_0}\right] && (7)\\
A_1(r) &= \Omega_0 r_0^2(1-\frac{\lambda}{2}\sin(\beta)\frac{R_1+R_2}{r_0}+\frac{e_1}{2}\cos(\theta_1)). && (8)
\end{aligned}
$$

Let us call δA the outward transport of angular momentum for one collision. Taking into account that particle #1 may be closer to the primary than #2 ($sin(\beta)>0$ as in Fig. 1) or farther out ($sin(\beta)<0$), we have:

$$
\delta A = -sign(sin(\beta))(A_1'-A_1) \tag{9}
$$

where primes denote after–collision quantities. The transport of angular momentum per unit of time is:

$$
\begin{aligned}
\frac{dA}{dt} &= \int_{e_2} de_2\int_{\theta_2} d\theta_2\int_{e_1} de_1\int_{d\theta_1} d\theta_1 n(e_2,\theta_2)n(e_1,\theta_1)\\
&\quad\times\int d\beta(R_1+R_2)|V_v|\int_{\min(r(0),r(1))}^{\max(r(0),r(1))}\delta A(r)2\pi r dr\\
&= \int_{e_2} de_2\int_{\theta_2} d\theta_2\int_{e_1} de_1\int_{d\theta_1} d\theta_1 n(e_2,\theta_2)n(e_1,\theta_1)\\
&\quad\times\int d\beta(R_1+R_2)|V_v|2\pi\int_0^1 d\lambda|\sin(\beta)|(R_1+R_2)r(\lambda)\delta A(\lambda)\\
&= \int_{e_2} de_2\int_{\theta_2} d\theta_2\int_{e_1} de_1\int_{d\theta_1} d\theta_1 n(e_2,\theta_2)n(e_1,\theta_1) && (10)\\
&\quad\times\int d\beta(R_1+R_2)^2\Omega_0 r_0^2 2\pi r_0(-\sin(\beta))|V_v|(\frac{e_1'}{2}\cos(\theta_1')-\frac{e_1}{2}\cos(\theta_1)).
\end{aligned}
$$

Note that to first order in e, $r(\lambda)\delta A(\lambda)$ is actually independent of λ.

From numerical evaluation of (10), we can calculate the non–local angular momentum transport and hence the viscosity.

III Results for single-size particles in a flat ring

Our first numerical experiments were applied to a two-dimensional ring with particles all of a single size. Initial conditions were selected with a distribution of orbital eccentricities at a distance of 10^5 km from a Saturn-mass primary, such that there is a linear decrease of the number of bodies with each e value, from a maximum at $e = 0$ to zero at some selected value. Usually the initial maximum e is about 2×10^{-7}, corresponding to er_0 being about 20m. The initial conditions also have the particles at any point being uniformly distributed in mean anomaly θ, i.e. the longitudinal distance from their own pericenters. Each of the cases explored in this paper reached a steady state after about 2 hours of CPU time on an HP 735/99 computer independent of the optical depth.

As discussed by Greenberg (1988), the distribution in (e, θ) maps directly into (V_r, V_t) space. The coordinates eccentricity e vs. mean anomaly θ are essentially polar coordinates equivalent to local velocity coordinates, as defined by Ojakangas and Greenberg. A population of particles with a single e value and a uniform distribution in θ would be distributed in (V_r, V_t) space along ellipses with a 2:1 axis ratio, elongated in the V_r direction. Particles with $\theta = 0$ lie on the $+V_t$ axis, those with $\theta = \pi/2$ lie twice as far from the origin on the $+V_r$ axis, etc.

Fig. 2a shows the initial distribution for a case with two-meter radius particles in a disk with optical thickness $\tau = 1$. This case is similar to conditions in Saturn's A and C rings (Marouf et al. 1983), where most of the mass is due to particles several meters across with optical thickness of those particles approaching unity (although most of the total optical depth is due to much smaller particles that play a less important role in the dynamics).

Fig. 2b shows the distribution after about half an orbital period. The particle distribution has clustered at values of θ that correspond to positive values of $V_r V_t$, consistent with previous evaluations of this distribution. Remarkably, the distribution shown in Fig. 2b is already almost a steady-state; Several orbits later there is negligible further change. This rapid evolution to the steady state is consistent with analytical estimates of collision rates that carefully account for collision cross-sections (eg. Ojakangas and Greenberg, 1990). (A conventional rule of thumb that collision frequencies are roughly 2τ per orbit gives too low a rate.)

The average velocity and angular momentum transport in this steady state are summarized in Table 1. This first case appears on the first line with $\tau = 1$ (the fifth line of data in Table 1.). The thermal velocity ($9 \times 10^{-4} m/s$) is almost five times larger than that required for a steady-state in Goldreich and Tremaine's (GT) model ($2 \times 10^{-4} m/s$). By itself, this change in V inserted into the GT theory would yield an increase in the kinematic viscosity by a factor proportional to V^2, i.e. about twenty, as seen in comparing column ν_{GT} ($1.7 \times 10^{-5} m^2/s$) with ν'_{GT} ($3.3 \times 10^{-4} m^2/s$). When we compute the viscosity from the local mass transport in our steady-state population (Fig. 2b), we get a similar, but somewhat larger, value $\nu_{local} = 4.1 \times 10^{-4} m^2/s$. The non-local viscosity is yet an order of magnitude higher, $2.8 \times 10^{-3} m^2/s$.

It is certainly reasonable that inclusion of the non-local component of viscosity would increase the total viscosity. However, non-local effects are also responsible for the increase in V, because particles can reach across the shear boundary, collide, and convert shear velocity into eccentric motion. Thus the steady-state velocity distribution itself is modified by the non-local effects. As a consequence, even what we have called the local viscosity is modified by non-local effects, to the extent that the velocity distribution is affected.

An important caveat regarding these results is that they are based on the two-dimensional model. As shown in Table 1, in this case ae is almost four times larger than the particle radius. In a real planetary ring, partitioning of collisional energy out of the plane would produce ring thickness comparable to ae, so the validity of the 2D model becomes marginal. However, as shown in Sec. IV, when modifications are made to the model to account for ring thickness, the trends found in this first case are confirmed, even more strongly.

Next consider a similar case except that ϵ is assumed to be fixed at a value of 0.4, rather than dependent on V. According to the GT model, for $\tau = 1$, a fixed ϵ of that value would result in indefinite decrease in average V, with no steady-state viscosity value. Figs. 3a,b,c show a time sequence in such a case. From the initial state in Fig. 3a, after half an orbital period (t=3 in Fig. 3b) the distribution is nearly at the steady state (Fig. 3c). Results are summarized on line 11 of Table 1. The mean V has only dropped to a value slightly smaller that in the case of variable ϵ. Here ae is very close to the particle diameter, so it is already outside the range of validity of the GT model. The finite size of the particles sets a lower limit on the damping of random velocity, which is evident because we have included non-local effects. Viscosity values are similar to those computed in the previous case; again the non-local component of viscosity is dominant.

As shown in Table 1, cases with ϵ fixed at lower values, 0.1 and 0.3, lead to very similar distributions. Again, V damps to a value controlled by the particle size such that ae is comparable to R. V and computed viscosity values are similar to those obtained for $\epsilon = 0.4$.

Changing the fixed value of ϵ to 0.5 yields the sequence shown in Figs. 4a,b,c. Here random velocities quickly increase to high values. By 5% of an orbital period (Fig. 4b), most particles, which originally had ae less than $\sim$ 4m, have $ae > 10$m. During the next several periods, the remainder of the particles have ae pumped up to > 10m (Fig. 4c). According to these results, the critical value of epsilon for a steady state is between 0.4 and 0.5, considerably lower than the value ~ 0.8 found by earlier studies.

Steady state results for other cases with $R = 2$m are shown in Figs. 5 and 6, where ϵ depends on V as in Fig. 2a-b, but here τ is 0.1 and 10, respectively. Numerical results for these cases are given in Table 1, including also the case with $\tau = 0.01$. In all these cases, viscosity is considerably larger than the local component. For larger τ, the non-local component of viscosity becomes overwhelming. For smaller τ, collisions are relatively infrequent, so a large part of the momentum transport is expected to be due to particles crossing the shear boundary; Table 1 shows that the non-local part is not dominant (although still very important) for small τ. Even in the case of low τ, we are finding total kinematic viscosity 50 times larger than given by the GT model, for example.

Another meaningful trend is seen in the comparison of Figs. 5 and 6, showing why local viscosity decreases both for very large and very small τ (a result first found by GT). For low τ, Greenberg (1988) showed that particles should be widely distributed in θ with modest concentrations near $\theta = 45°$ and 225°, such that local viscosity (recall proportional to $\langle V_r V_t \rangle$) is small. This result is clearly demonstrated in Fig. 5. At the opposite extreme of large τ, concentrations in the θ distribution are stronger, but viscosity is limited because the concentrations are only slightly above $\theta = 0°$ and 180°.

Results discussed so far all assumed particle radii of 2m. Table 1 also shows results for smaller particles. For $R = 20$cm, V is reduced by a factor ~ 5 relative to the 2m cases for the same τ. These values, as well as the local viscosity, are fairly close to the GT values, which are independent of particle size. This closer agreement with GT for smaller bodies probably reflects the diminished importance of particles' physical extent in converting keplerian shear to random motion.

For still smaller particles (see the cases with $R = 1$cm in Table 1), several of the trends discussed above continue to hold. For $\tau \ > 1$ the non-local viscosity remains very important, but for smaller τ, the non-local viscosity becomes less than the local component, the only place on Table 1 where that occurs. Note however that for these small particles, the steady state random motion is such that ae is typically $>$ 30 times the particle size. Because random motion would be partitioned to include out-of-plane motion, the two-dimensional model is probably only relevant for real planetary rings where particles with $R > 20$cm dominate dynamical processes. Moreover, it must be recognized that any results for the case $\tau > 1$ are artificial in a two-dimensional case.

IV Three-dimensional cases

In order to evaluate the effect of significant ring thickness, we have modified our numerical model in the following way. We account for collisional partitioning of random motion between in-plane and out-of-plane components by taking the ring thickness h to be equal to $2ae$. We again model each particle as a cylinder, with its axis perpendicular to the orbital plane, but now we assume that the length of the axis is equal to the diameter $2R$ of the particle. This allows us to reduce the collision frequency by a factor $2R/h$. In all other ways the algorithm remains as in the 2D model. Although the vertically aligned cylinders do not allow for modelling of exchange between in-plane and out-of-plane motion, the assumption of equiparition is reasonable and the cylinder do allow us to account for the less well-understood in-plane transport processes.

Results using this three-dimensional model are shown in Table 2. In addition, the viscosity values are shown graphically in Fig. 7. We consider the cases in the same order as they were discussed in Section III. For $\tau = 1$ and $R = 2$m, with the velocity-dependent ϵ, we find that the steady-state random velocity is nearly twice what we found with the 2-D algorithm, giving a comparable increase in the local viscosity (both versions, ν'_{GT} and ν_{local}). However, the non-local viscosity decreases by a factor of 5 relative to the 2-D model, because of the reduced impact rate in the thicker disk. The local viscosity is about 40 times that given by the GT theory, and the non-local component doubles the mass transport above the local component alone.

Next we considered the effect of using a fixed value of epsilon, still with $\tau = 1$ and $R = 2$m. As in the 2D case, we confirm that sufficiently large

ϵ values lead to indefinite increase in random velocity and in corresponding values of ae (e.g. for $\epsilon = 0.6$); smaller ϵ values (e.g. the case $\epsilon = 0.5$ shown in Table 2) lead to values of ae comparable to the particle size. The critical ϵ value for a steady state is between 0.5 and 0.6, larger than given by the 2D calculations, but still less than the equilibrium value $\epsilon = 0.8$ found by GT in their model (with local-viscosity only).

Exploring the effects of varying τ for a fixed particle size $R = 2$m, we find similar trends to the 2D models. Viscosity is considerably larger than ν_{GT}, especially for larger τ. However, the values are not as extreme as in the 2D case. For small τ the total viscosity is only a few times larger than ν_{GT}, while for $\tau = 10$, it is still several orders of magnitude larger.

For $R = 20$cm, the local viscosity values are comparable to the 2D results. The non-local component is much smaller than found with the 2D model: For $\tau \leq 1$, it is negligible compared to the local component, but for $\tau = 10$ it is much larger than the local component and 100 times larger than ν_{GT}.

For cm-size particles, where $ae >> R$, we expected the 2D results to be invalid. The 3D model does give very different results. In general the non-local viscosity is small compared with the local component, and the local component is comparable to ν_{GT}.

V Conclusions

Our computations of angular momentum transport in planetary rings, taking into account the role of the finite sizes of particles, confirms significant effects on the relative velocity distribution among colliding particles and on transport processes, due to collisions between particles whose centers are at different distances from the central planet. The latter effect is responsible for the non-local component of the viscosity. The various trends of interest are apparent in Fig. 7.

Generally, the rms random velocity appears to be quite close to the value based on Goldreich and Tremaine's original theory for cases with the smallest particle sizes (cm-scale). This result can be seen comparing the velocity values in Table 2, or by comparing ν_{GT} and ν'_{GT} in Table 2 or Fig. 7. (The difference between those two viscosity values is due only to the difference in random velocity.) On the other hand, the velocity values we find for multi-meter particles is a few times larger than the GT value. This result is reasonable: A model that accounts for the finite size of particles would in fact be expected to be most relevant for larger particles rather than for small particles, which can be approximated by infinitesimal sizes.

Similarly, computations of momentum transport, as characterized by the kinematic viscosity components ν_{local} and $\nu_{non-local}$, show greatest deviation from the GT results for the larger bodies. Evidently the ability to reach radially and transmit momentum during a collision is most effective for larger bodies. Even the local component is affected by the finite particle size because of the effect on the random velocity. There is also a strong and not unexpected correlation with optical thickness τ: the greater frequency of collisions with larger τ means that a proportionately greater contribution to momentum transport comes during collisions than during the free radial motion of particles, which was assumed dominant process in the GT theory.

Fig. 7 shows that, although ν_{total} increases with τ for larger particles, it decreases strongly for cm-size particles as τ increases above 1. That result seems to support Salo's (1991) suggestion that the ringlet instability mechanism may be possible for rings that are predominantly composed of the smaller particles.

Our results can also be compared with the many-particle simulations of Wisdom and Tremaine (1988) and of Salo (1991), which gave results very similar to one another. For the cases that they considered, with particle radii of 1m, we have computed and compared our own values of $\nu/\Omega R^2$ (c.f. Salo's Fig. 5c) with those given by Salo (Fig. 8). Note that the non-local component is in fairly good agreement, generally about 10% higher than the many-particle simulations. The results are remarkably consistent given the completely different calculational process. The local component also agrees very well for values of $\tau < 0.5$, but diverges substantially for larger τ. In general for all of these cases with $R = 1m$, the steady-state rms relative velocity among particles is about 20% higher in our calculations than in the many- particle simulations.

There are several possible reasons for the disagreement between our results especially for the larger values of τ. First, our three-dimensional model is really a corrected version of a two- dimensional calculation. More precise results will require a full three-dimensional calculation, which could still use our statistical approach. Second, our model does not include the effects of physical packing among particles which can occur when the filling factor (the fraction of space filled with the volume of particles) becomes high. This effect can in principle be included by modifying the statistical treatment, including restricting the range of possible collision geometries in a tightly packed system.

The computational technique introduced here provides insight into the statistical processes that determine viscosity, supplementing the results of direct numerical many-body simulations. Moreover, it has the potential for application to other interesting models. We plan to consider momentum transport in systems with two or more different sizes of particles for example. It will also be possible to examine the effects of gravitational interactions among particles, which may introduce a significant non-local component to the viscosity under some circumstances. Such results may be applicable to other dynamical systems, such as planetesimal populations during planet formation, as well as to known planetary rings. Such conditions are ideally suited for application of our technique, because the added features will involve very little additional computation time, and the low τ conditions are in the regime where our approach is strongest and where direct numerical simulations may be impractical. Non-local interactions, whether due to finite size of colliding bodies or mutual gravitation clearly play an important role in momentum transport in a variety of kind of astronomical disks.

Acknowledgments

We are grateful for help and comments by Dan Durda, Joe Plassmann, Jyrki Hanninen, and Michel Henon. Thoughtful reviews by Glen Stewart and Heikki Salo were also valuable. The research reported here was done during Jean-Marc Petit's extended visit to the Lunar and Planetary Laboratory, on leave from the Observatoire de Nice. This work was supported by NASA's Planetary Geology and Geophysics program.

References

Araki S., and Tremaine S. 1986. The dynamics of dense particle disks. *Icarus* **65,** 83– 109.

Bridges, F.G., Hatzes, A., and Lin, D.N.C. 1984. Structure, stability, and evolution of Saturn's rings. *Nature* **309,** 333– 335.

GOLDREICH P., AND TREMAINE S. 1978. The velocity dispersion in Saturn's rings. *Icarus* **34,** 227– 239.

GREENBERG, R. 1988. Particle properties and the large-scale structure of planetary rings: Rebound characteristics and viscosity. *Icarus* **75,** 527– 539.

OJAKANGAS G.W., AND GREENBERG R. 1990. Viscosity and mass transport in nonuniform keplerian disks. *Icarus* **88,** 146– 171.

SALO, H. 1991. Numerical simulations of dense collisional systems. *Icarus* **90,** 254– 270.

SHU, F.H., AND G.R. STEWART 1985. The collisional dynamics of particulate disks. *Icarus* **62,** 360– 383.

WISDOM, J. AND S. TREMAINE 1988. Local simulations of planetary rings. *Astron. J.* **95,** 925– 940.

Figure Captions

Figure 1 Geometry of impact between two finite-sized particles centered at different distances from a planet. The vertical dashed line just to the right of the center of particle #1 is the shear boundary under consideration and lies along a constant radial distance from the planet.

Figure 2 (a) Initial velocity distribution for a case with two-meter- radius particles in a two-dimensional ring with optical thickness $\tau = 1$, represented by eccentricity and mean anomaly, which map directly into (V_r, V_t). (b) The steady-state distribution reached after only half an orbital period.

Figure 3 A time sequence (a,b,c) showing the evolution of the velocity distribution in a case where the coefficient of restitution ϵ is less than the critical value for equilibrium. Velocities damp to a steady-state governed by particle size.

Figure 4 A time sequence (a,b,c) showing the evolution of the velocity distribution in a case where the coefficient of restitution ϵ is greater than the critical value for equilibrium. Velocities increase indefinitely.

Figure 5 Steady-state result for $\tau = 0.1$ shows expected clustering near $\theta = 45°$ and $225°$, as discussed by Greenberg (1988).

Figure 6 Steady-state result for $\tau = 10$ shows expected clustering near $\theta = 0°$ and $180°$.

Figure 7 Viscosity values for cases shown in Table 2. All cases shown are for the velocity-dependent ϵ, and the dot sizes correspond to the particle radii in Table 2 (smallest dot is for R = 1cm, largest is for R = 2m). Note the decrease in ν_{GT} as τ increases above 1, which would imply the possibility of ringlet instability. The difference in values between ν_{GT} and $\nu\prime_{GT}$ indicates the effect of the different velocities found in our calculations relative to Goldreich and Tremaine's theory. The GT theory yields the local component of viscosity only, and can be compared with our results in the column labeled ν_{local}. The total viscosity for each case is shown in the last column, which is the sum of the last two columns in Table 2 (ν_{local} plus $\nu_{non-local}$). The right hand column of this figure

(ν_{total}) shows that only for the cm-scale particles does ν decrease with increasing τ, so as to drive ringlet instabilities.

Figure 8 Comparison of viscosity values found for a set of cases explored in the many-body simulations of Salo (1991) and recomputed by our statistical method. The local component differs significantly for $\tau > 0.5$, but the non-local component agrees remarkably well.

τ	ϵ	R	ae	our V	V_{GT}	ν_{GT}	ν'_{GT}	ν_{local}	$\nu_{non-local}$
.01	V	2.	11.	1.36×10^{-3}	5×10^{-4}	2×10^{-6}	1.52×10^{-5}	4.55×10^{-5}	3.24×10^{-5}
.1	V	2.	11.	1.35×10^{-3}	5×10^{-4}	2×10^{-5}	1.48×10^{-4}	3.73×10^{-4}	3.65×10^{-4}
.1	V	.2	2.4	3.02×10^{-4}	5×10^{-4}	2×10^{-5}	7.42×10^{-6}	3.12×10^{-5}	1.27×10^{-5}
.1	V	.01	.54	6.65×10^{-5}	5×10^{-4}	2×10^{-5}	3.60×10^{-7}	1.34×10^{-6}	3.46×10^{-7}
1.	V	2.	7.2	8.95×10^{-4}	2×10^{-4}	1.7×10^{-5}	3.29×10^{-4}	4.14×10^{-4}	2.81×10^{-3}
1.	V	.5	2.5	3.12×10^{-4}	2×10^{-4}	1.7×10^{-5}	4.01×10^{-5}	5.29×10^{-5}	2.89×10^{-4}
1.	V	.2	1.2	1.54×10^{-4}	2×10^{-4}	1.7×10^{-5}	9.76×10^{-6}	1.07×10^{-5}	6.11×10^{-5}
1.	V	.01	.34	4.23×10^{-5}	2×10^{-4}	1.7×10^{-5}	7.37×10^{-7}	2.21×10^{-7}	1.09×10^{-6}
1.	.1	2.	4.1	5.13×10^{-4}			1.08×10^{-4}	1.42×10^{-4}	1.19×10^{-3}
1.	.3	2.	5.4	6.67×10^{-4}			1.86×10^{-4}	2.66×10^{-4}	1.85×10^{-3}
1.	.4	2.	6.3	7.79×10^{-4}			2.50×10^{-4}	3.64×10^{-4}	2.35×10^{-3}
10.	V	2.	6.0	7.41×10^{-4}	1×10^{-4}	8×10^{-7}	4.47×10^{-5}	2.46×10^{-4}	2.27×10^{-2}
10.	V	.2	1.0	1.28×10^{-4}	1×10^{-4}	8×10^{-7}	1.34×10^{-6}	5.96×10^{-6}	4.71×10^{-4}
10.	V	.01	.30	3.78×10^{-5}	1×10^{-4}	8×10^{-7}	1.16×10^{-7}	1.18×10^{-7}	8.23×10^{-6}

Table 1: Summary of results for the two-dimensional model in mks units (viscosities are in m^2/s). Column "τ" shows the optical thickness; "ϵ" shows the coefficient of restitution, with V indicating a velocity-dependent value based on the experimental results of Bridges et al. (1984); "R" shows the particle radius in meters; "our V" shows the RMS magnitude of velocity vector (V_r, V_t); "ae" shows the value of ae corresponding to "our V", for comparison with R; "V_{GT}" shows the RMS velocity according to the theory of Goldreich and Tremaine (1978, "GT"), such that the corresponding value of ϵ (from Bridges et al., 1984) gives a steady-state; "ν_{GT}" shows the corresponding kinematic viscosity according to GT's theory. "ν'_{GT}" is found by inserting the value of "our V" into the GT theory (i.e. their Fig. 4), instead of the value of V used in the previous column; "ν_{local}" is based on our evaluation of the mass transport due to particles crossing the shear boundary in the steady-state population that evolves in our numerical model; "$\nu_{non-local}$" is based on our evaluation of the non-local transport as calculated according to the theory described in Section II.

τ	ϵ	R	ae	our V	V_{GT}	ν_{GT}	ν'_{GT}	ν_{local}	$\nu_{non-local}$
.01	V	2.	8.6	1.54×10^{-3}	5×10^{-4}	2×10^{-6}	1.95×10^{-5}	7.99×10^{-6}	6.37×10^{-6}
.01	V	.01	3.2	5.85×10^{-4}	5×10^{-4}	2×10^{-6}	2.81×10^{-6}	2.14×10^{-6}	2.11×10^{-10}
.1	V	2.	8.6	1.53×10^{-3}	5×10^{-4}	2×10^{-5}	1.90×10^{-4}	8.92×10^{-5}	6.53×10^{-5}
.1	V	.2	3.5	6.34×10^{-4}	5×10^{-4}	2×10^{-5}	3.27×10^{-5}	1.38×10^{-5}	7.29×10^{-7}
.1	V	.01	2.1	3.76×10^{-4}	5×10^{-4}	2×10^{-5}	1.15×10^{-5}	5.11×10^{-6}	3.83×10^{-9}
1.	V	2.	8.6	1.49×10^{-3}	2×10^{-4}	1.7×10^{-5}	9.11×10^{-4}	6.48×10^{-4}	7.46×10^{-4}
1.	V	.5	3.7	6.41×10^{-4}	2×10^{-4}	1.7×10^{-5}	1.69×10^{-4}	1.16×10^{-4}	5.42×10^{-5}
1.	V	.2	2.6	4.56×10^{-4}	2×10^{-4}	1.7×10^{-5}	8.52×10^{-5}	5.71×10^{-5}	1.04×10^{-5}
1.	V	.01	2.1	3.64×10^{-4}	2×10^{-4}	1.7×10^{-5}	5.45×10^{-5}	3.53×10^{-5}	1.62×10^{-7}
1.	.5	2.	10.2	1.78×10^{-3}			1.30×10^{-3}	6.95×10^{-4}	7.45×10^{-4}
10.	V	2.	6.3	9.06×10^{-4}	1×10^{-4}	8×10^{-7}	6.68×10^{-5}	4.76×10^{-4}	7.26×10^{-3}
10.	V	.2	1.2	1.73×10^{-4}	1×10^{-4}	8×10^{-7}	2.43×10^{-6}	1.51×10^{-5}	9.13×10^{-5}
10.	V	.01	.48	7.13×10^{-5}	1×10^{-4}	8×10^{-7}	4.13×10^{-7}	1.67×10^{-6}	5.21×10^{-7}

Table 2: Results for the three-dimensional model. See caption of Table 1 for definitions of quantities shown.

Fig. 1

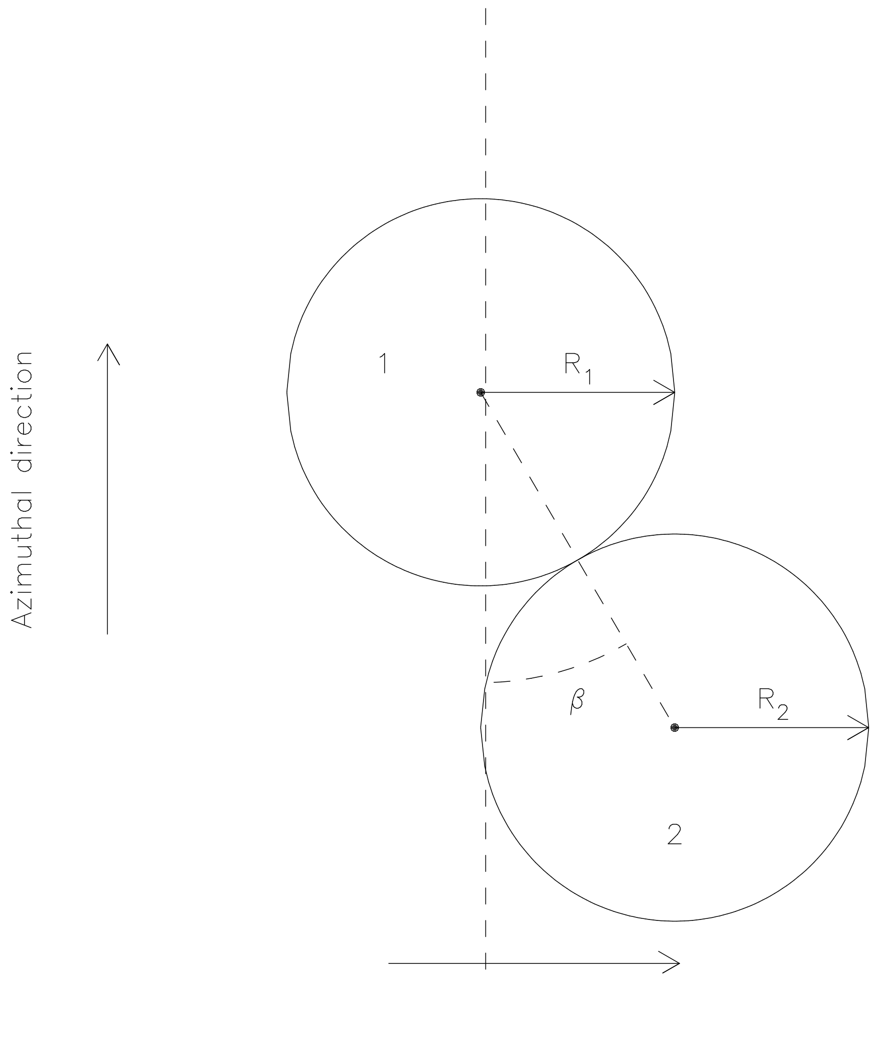

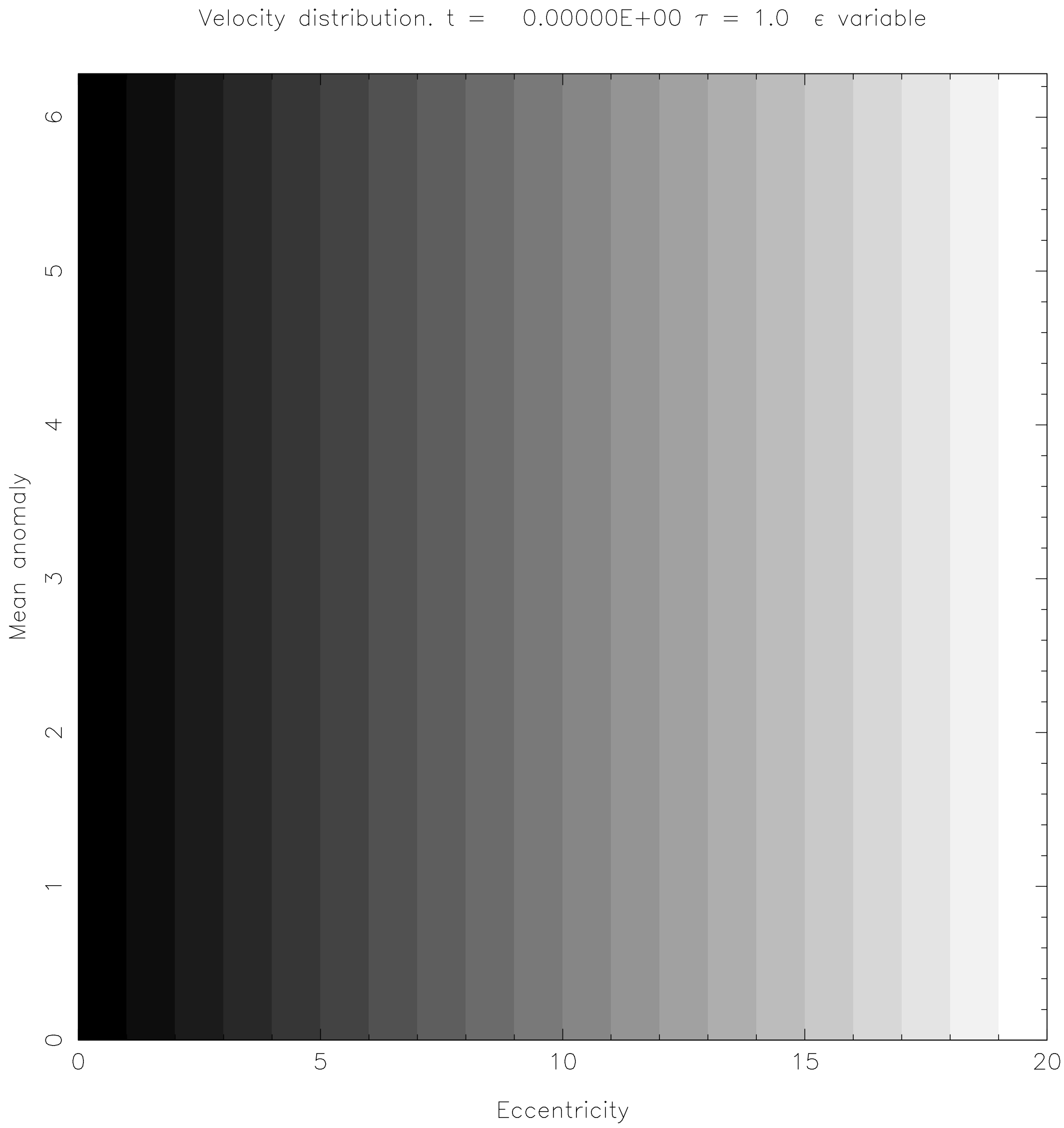
Velocity distribution. t = 0.00000E+00 τ = 1.0 ϵ variable
Mean anomaly
0
1
2
3
4
5
6
0
5
10
15
20
Eccentricity

Figure: 2a

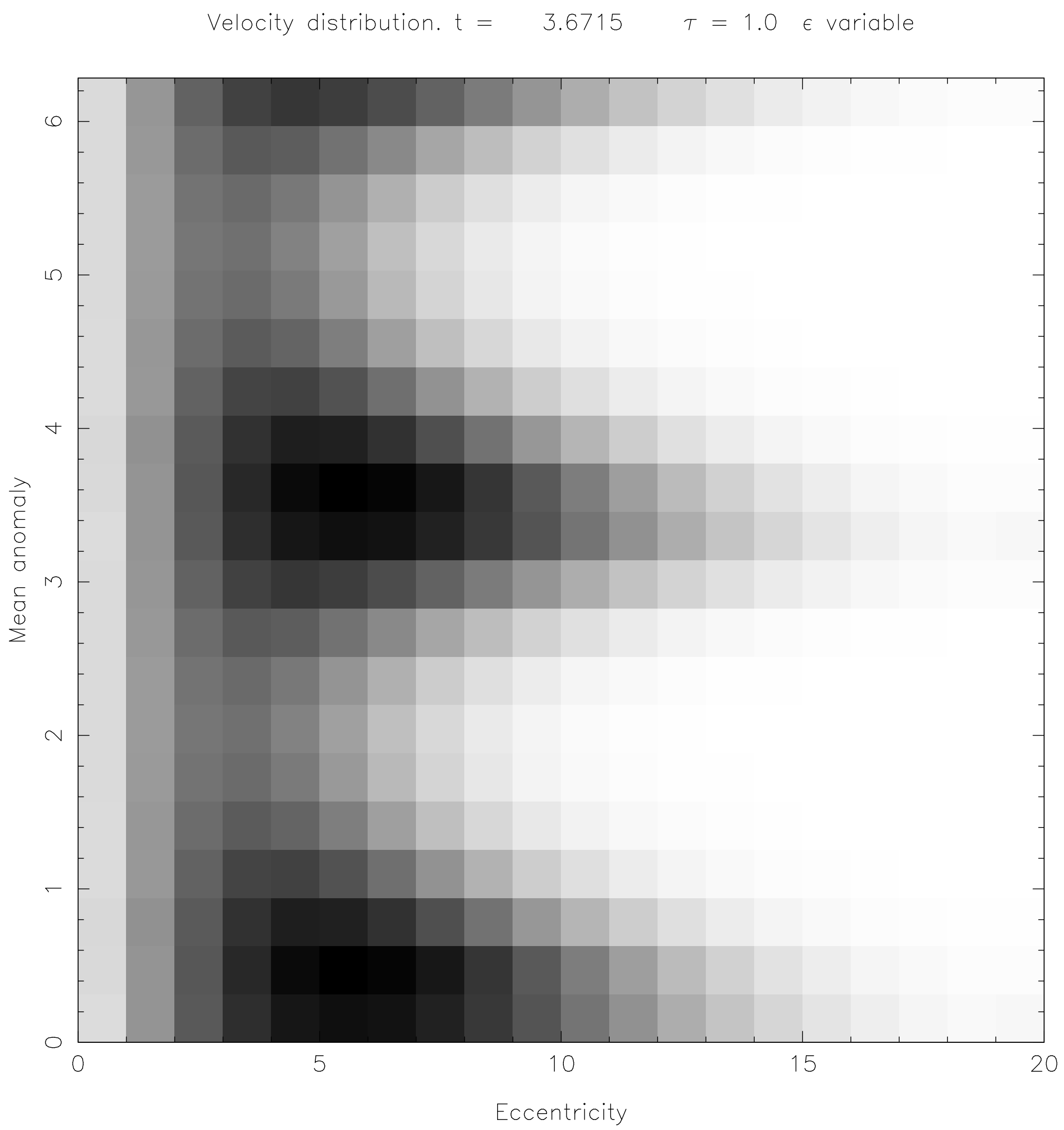
Velocity distribution. t = 3.6715 τ = 1.0 ϵ variable
Mean anomaly
0
1
2
3
4
5
6
Eccentricity
0
5
10
15
20

Figure: 2b

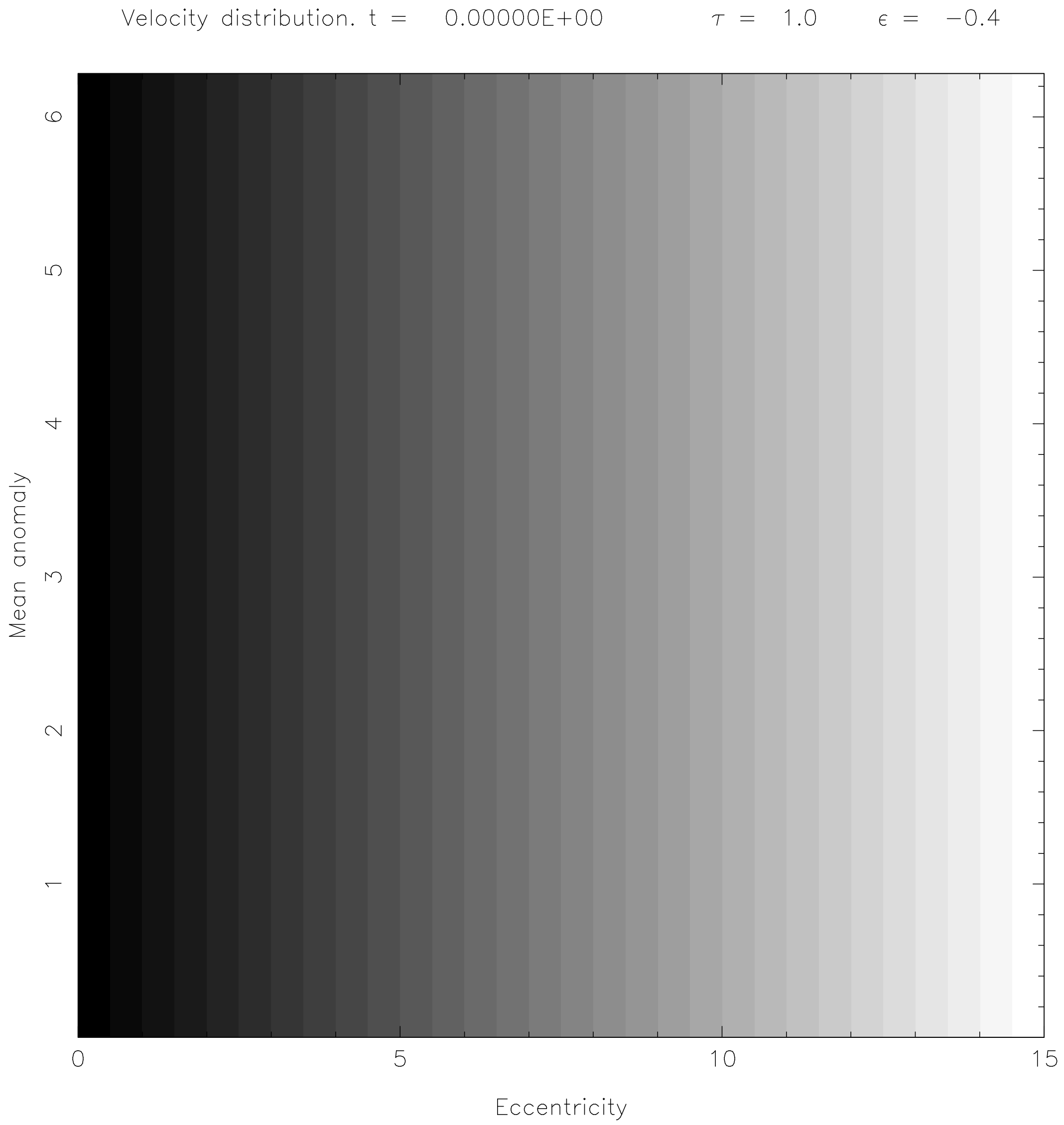

Velocity distribution. t = 0.00000E+00 τ = 1.0 ϵ = −0.4
Mean anomaly
6
5
4
3
2
1
0
5
10
15
Eccentricity

Figure: 3a

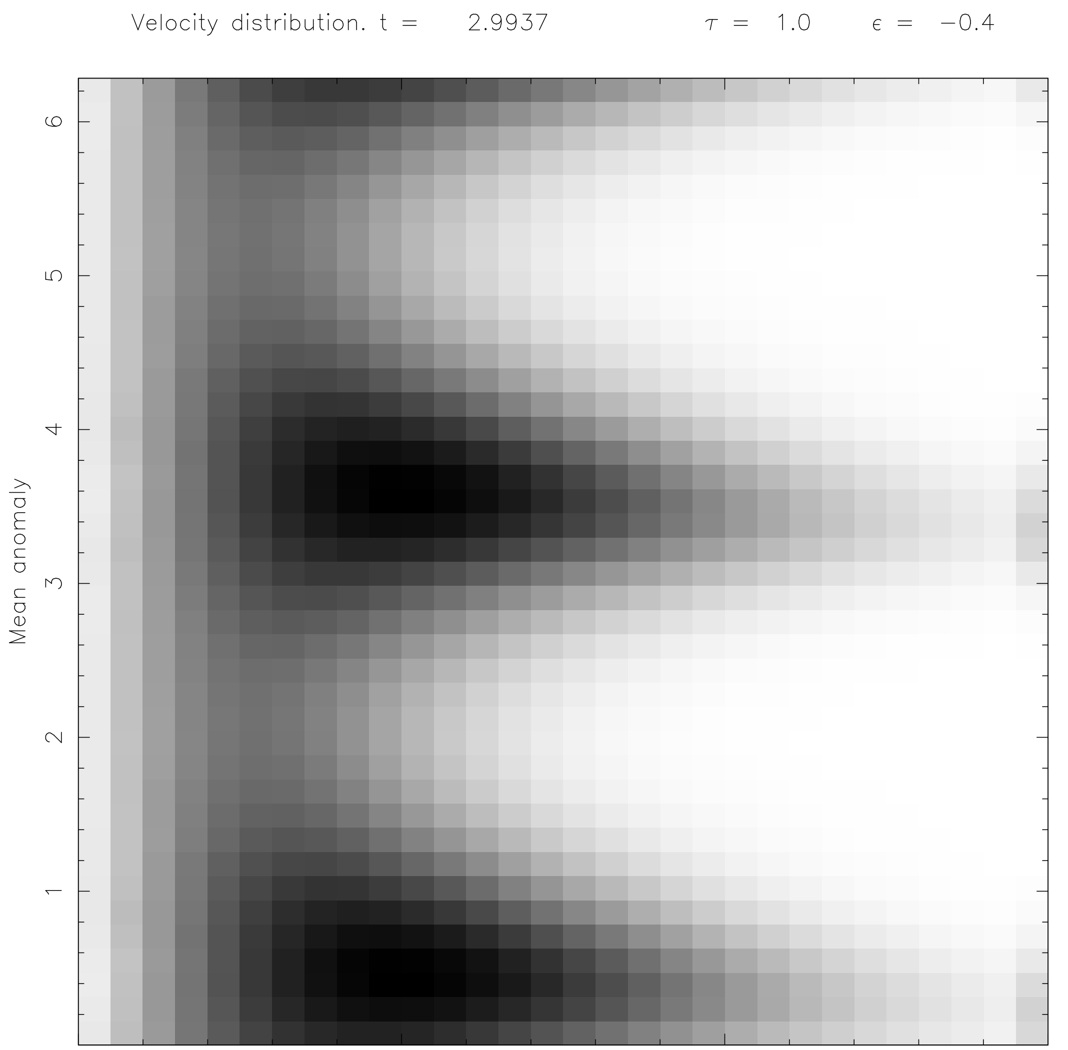
Velocity distribution. t = 2.9937 τ = 1.0 ϵ = −0.4
Mean anomaly
1
2
3
4
5
6
0
5
10
15
Eccentricity

Figure: 3b

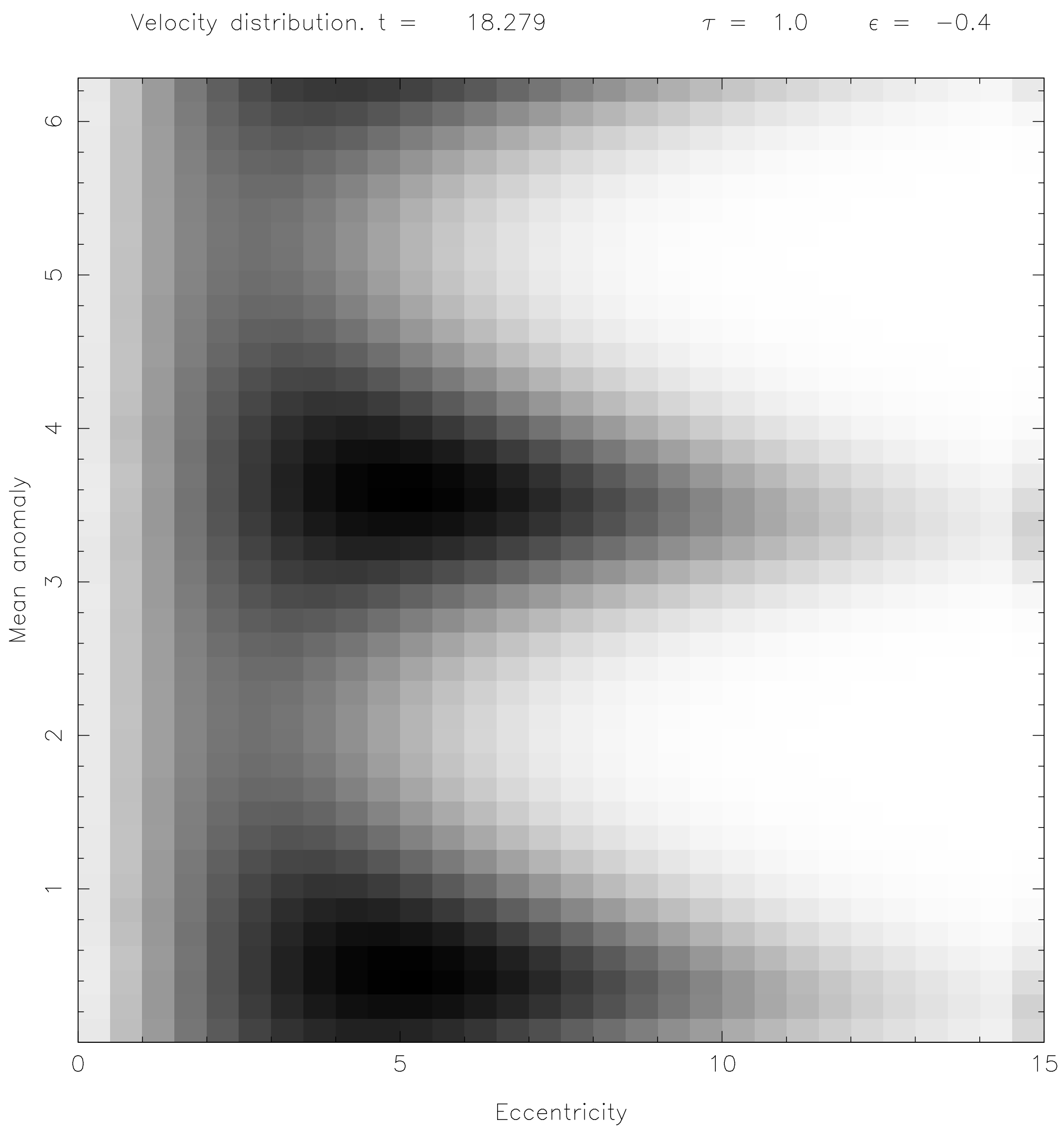
Velocity distribution. t = 18.279 τ = 1.0 ε = −0.4
Mean anomaly
Eccentricity
0
5
10
15
1
2
3
4
5
6

Figure: 3c

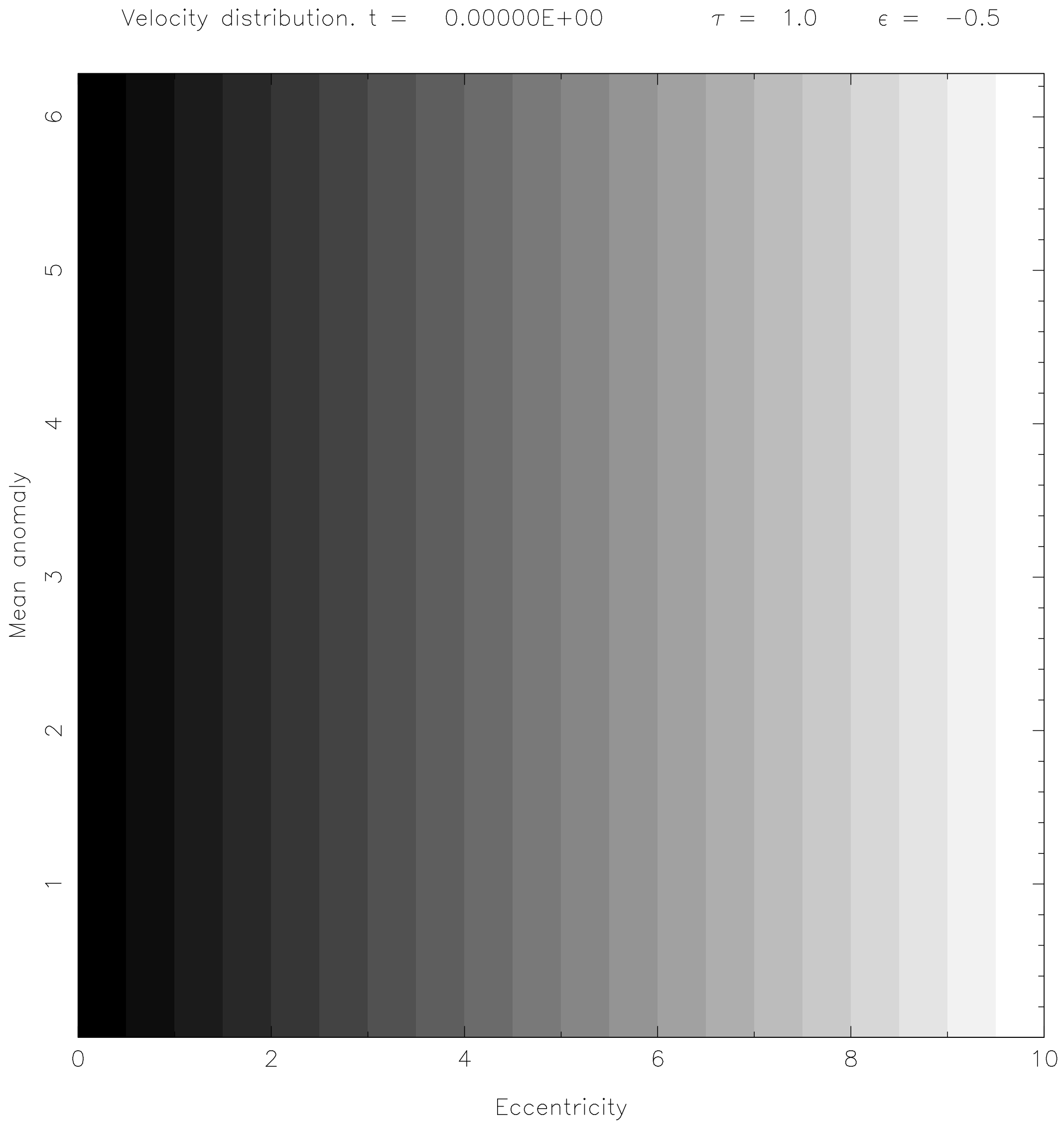
Velocity distribution. t = 0.00000E+00 τ = 1.0 ϵ = −0.5
Mean anomaly
1
2
3
4
5
6
Eccentricity
0
2
4
6
8
10

Figure: 4a

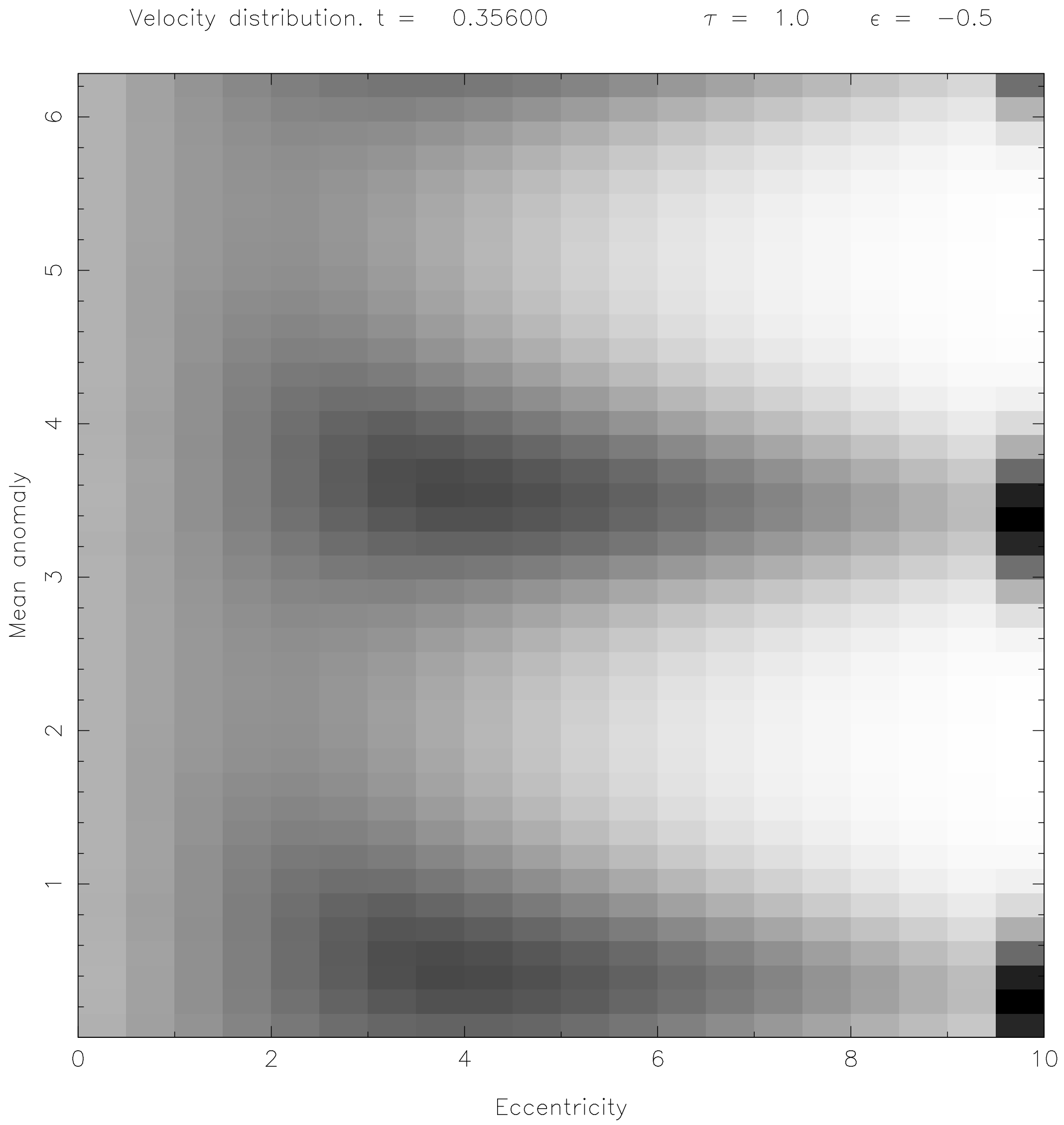
Velocity distribution. t = 0.35600
τ = 1.0
ϵ = −0.5
Mean anomaly
Eccentricity
0
1
2
3
4
5
6
0
2
4
6
8
10

Figure: 4b

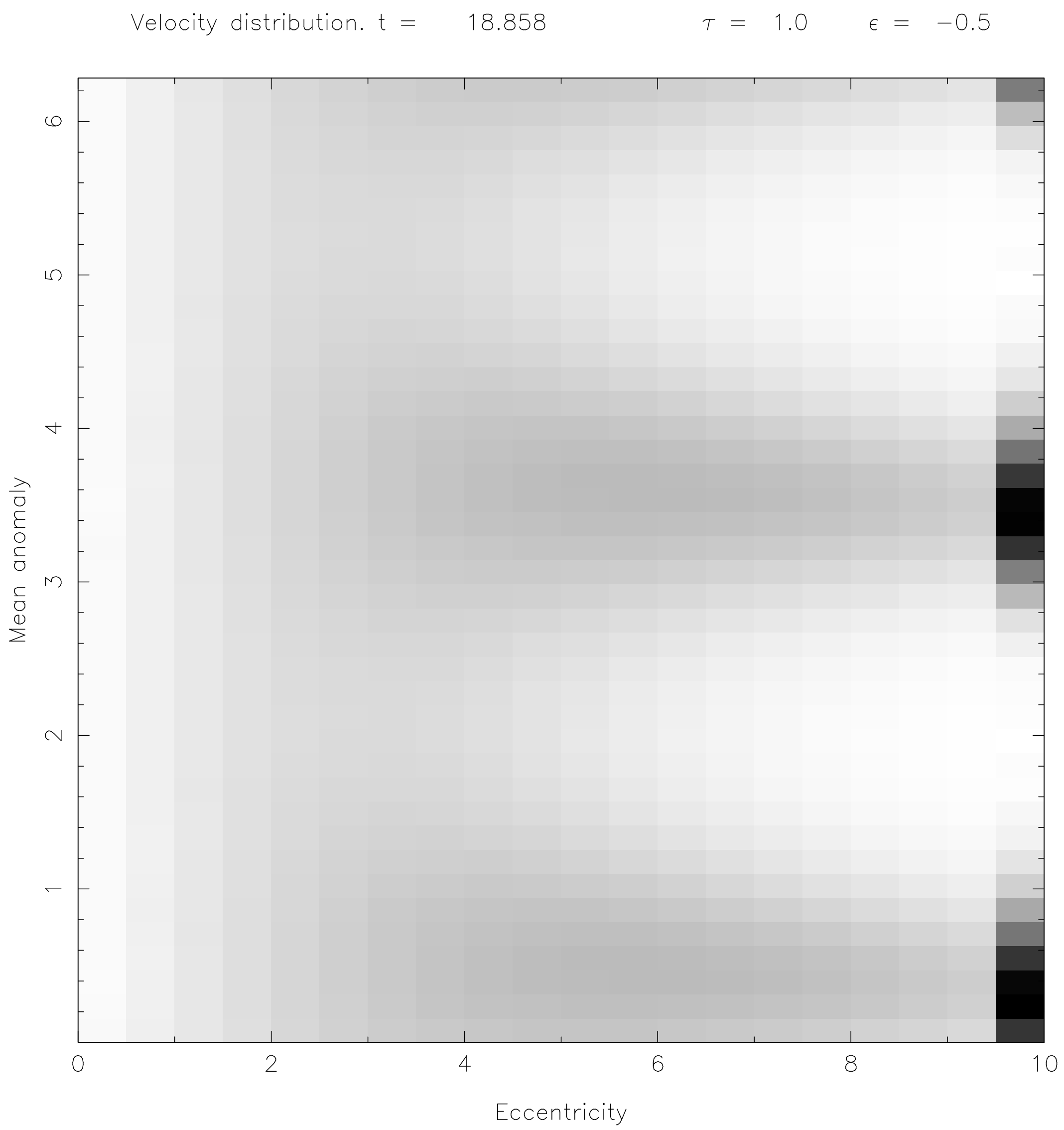
Velocity distribution. t = 18.858 τ = 1.0 ϵ = −0.5
Mean anomaly
Eccentricity
0
1
2
3
4
5
6
8
10

Figure: 4c

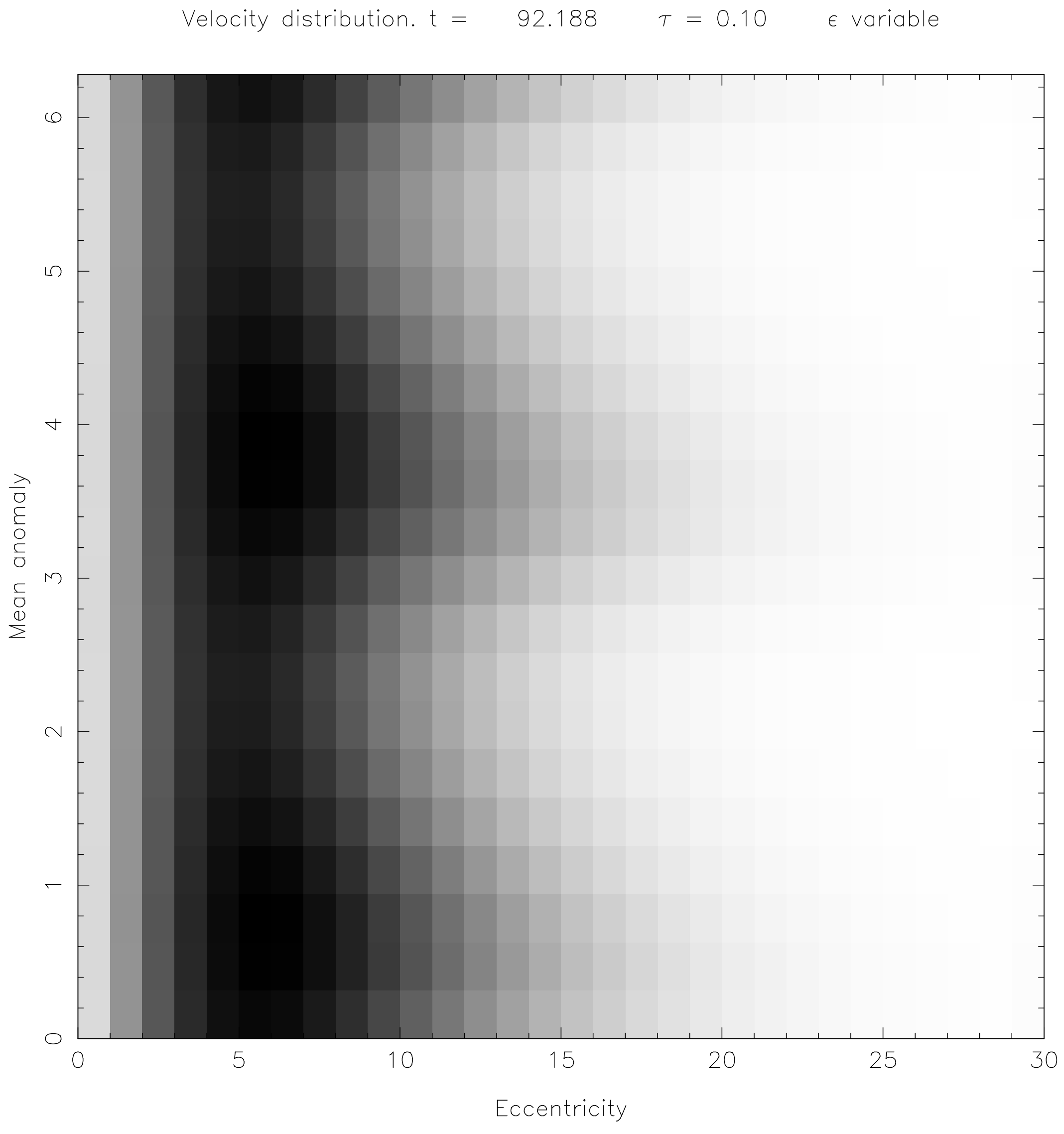
Velocity distribution. t = 92.188 τ = 0.10 ϵ variable
Mean anomaly
0
1
2
3
4
5
6
Eccentricity
0
5
10
15
20
25
30

Figure: 5

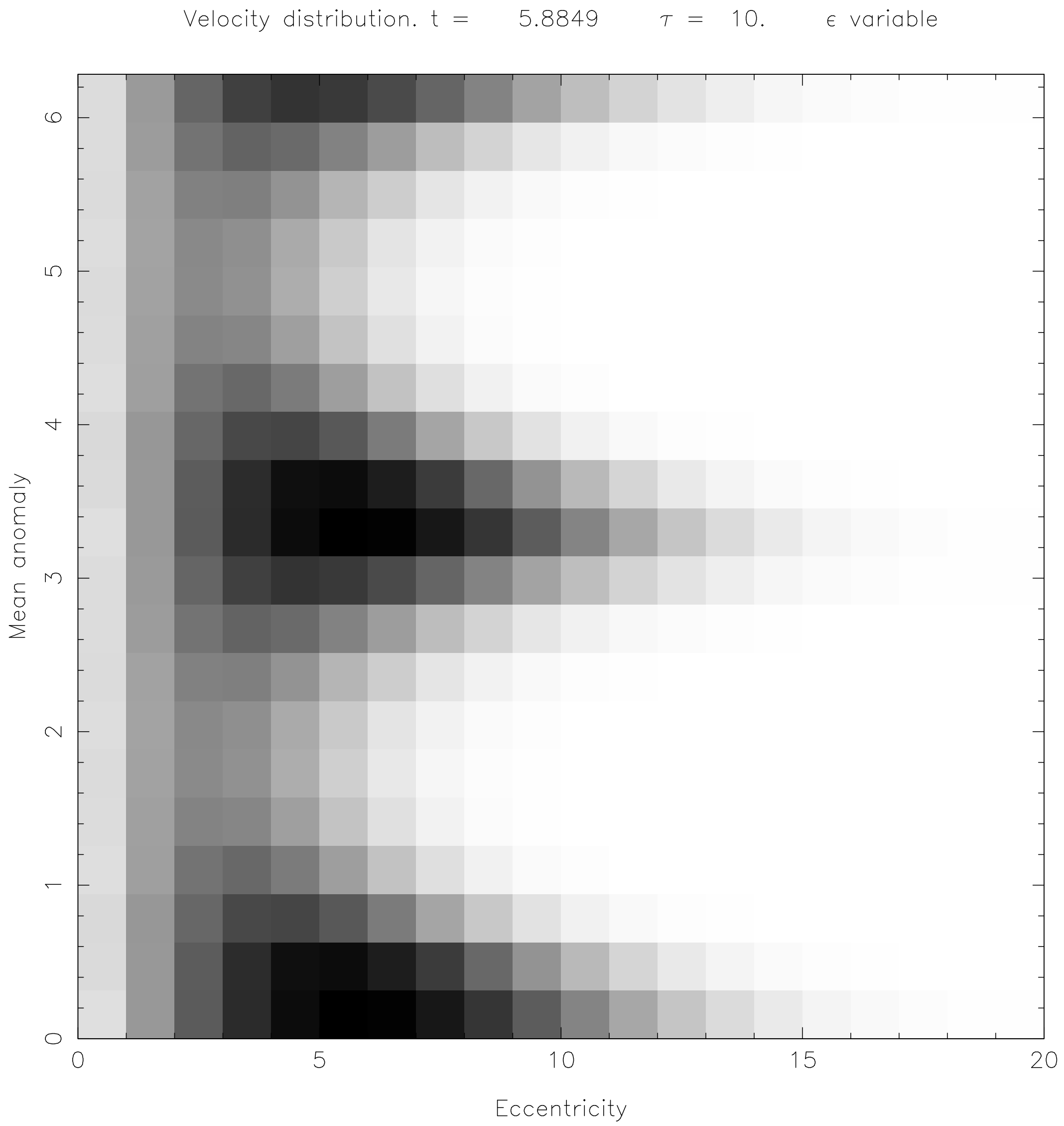
Velocity distribution. t = 5.8849 τ = 10. ϵ variable
Mean anomaly
0
1
2
3
4
5
6
0
5
10
15
20
Eccentricity

Figure: 6

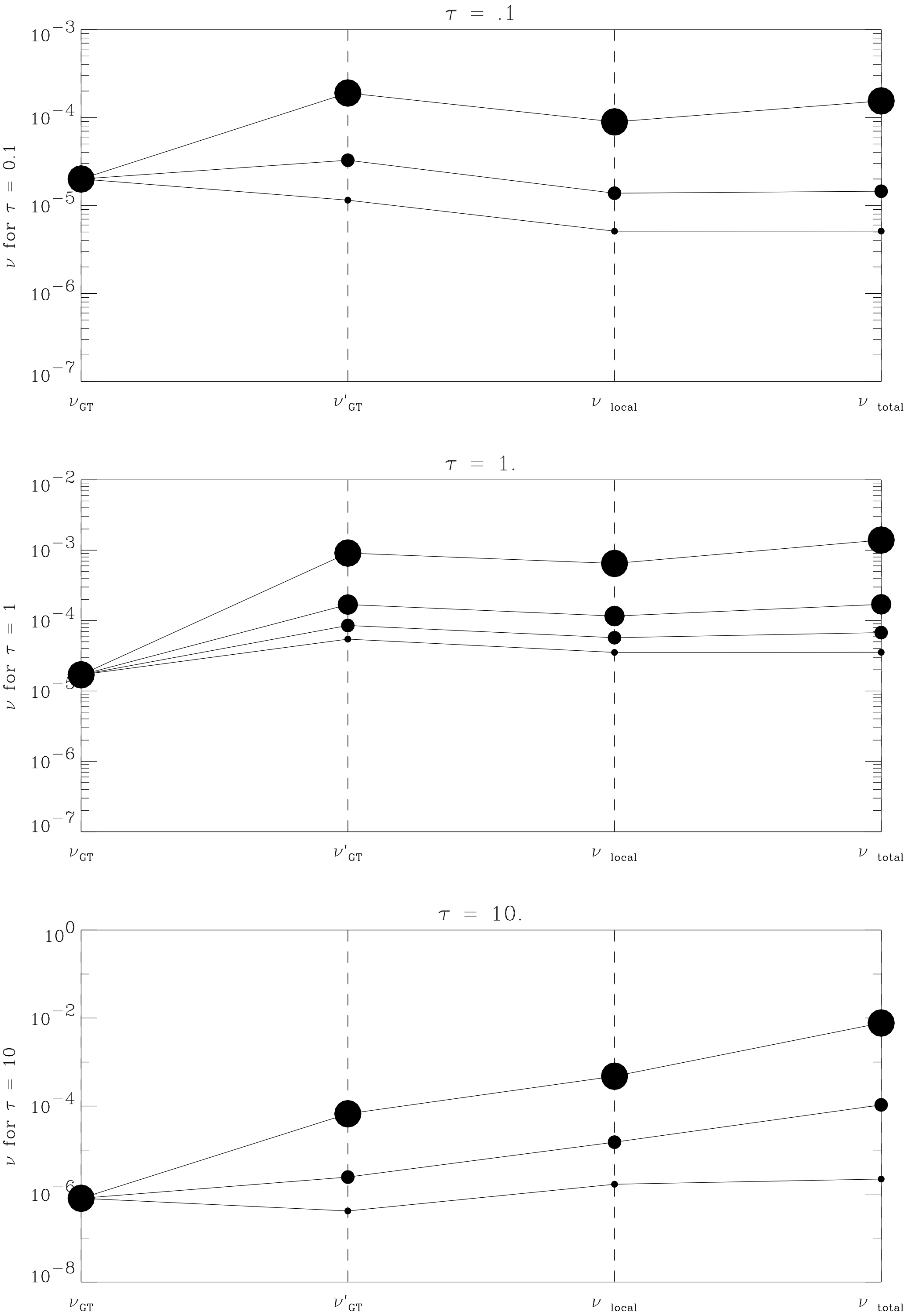
τ = .1
10^−3
10^−4
10^−5
10^−6
10^−7
ν for τ = 0.1
ν_GT
ν'_GT
ν local
ν total
τ = 1.
10^−2
10^−3
10^−4
10^−5
10^−6
10^−7
ν for τ = 1
ν_GT
ν'_GT
ν local
ν total
τ = 10.
10^0
10^−2
10^−4
10^−6
10^−8
ν for τ = 10
ν_GT
ν'_GT
ν local
ν total

Figure: 7

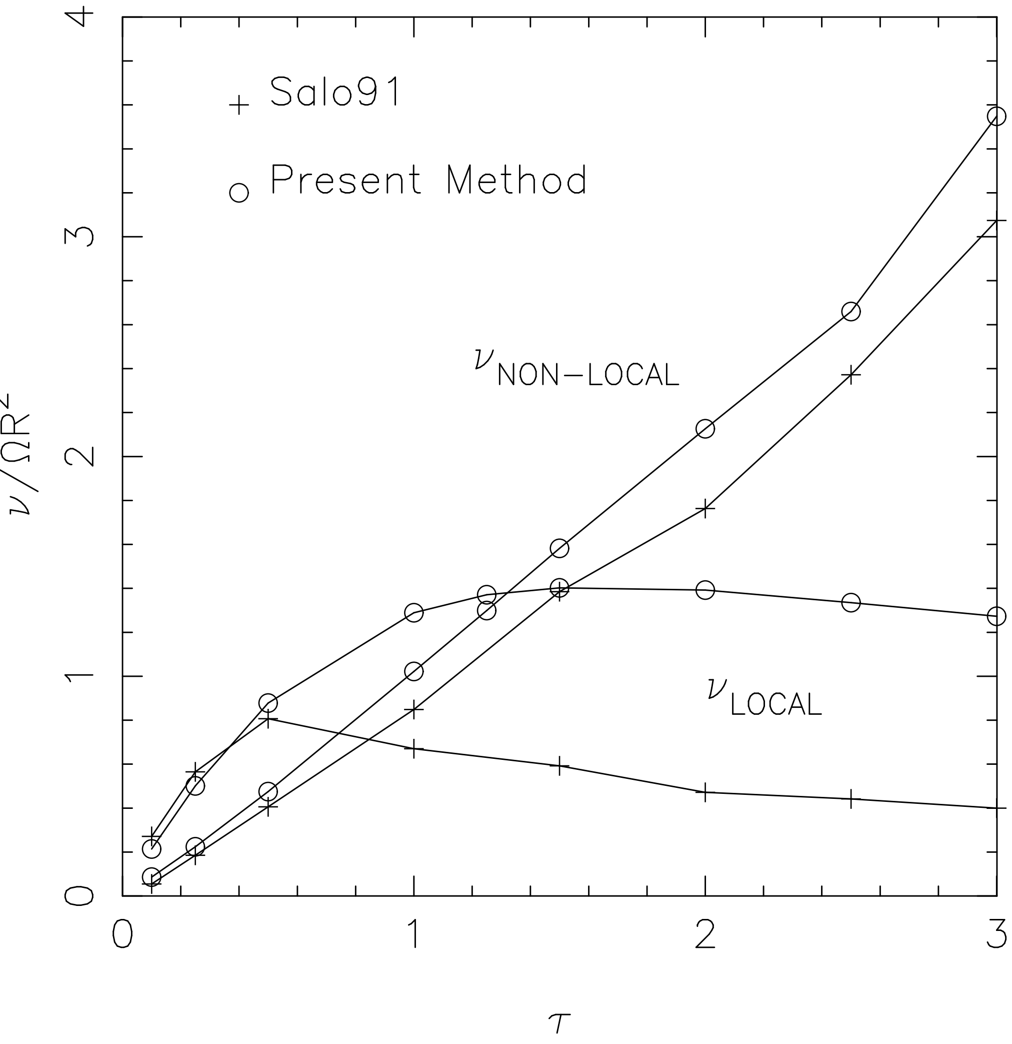

Salo91
Present Method
$\nu_{\mathrm{NON-LOCAL}}$
ν_{LOCAL}
$\nu/\Omega R^2$
τ
0
1
2
3
4

Figure: 8